Dalton Transactions

Nickel(II) Complexes Based on Dithiolate-Polyamine Binary Ligand Systems: Crystal structures, Hirshfeld surface analysis, Theoretical Study, and Catalytic Activity Study in Photocatalytic Hydrogen Generation

Journal:	*Dalton Transactions*
Manuscript ID	DT-ART-01-2021-000352.R1
Article Type:	Paper
Date Submitted by the Author:	10-Mar-2021
Complete List of Authors:	Adhikari, Suman; Govt. Degree College, Dharmanagar, Chemistry Bhattacharjee, Tirtha; Bineswar Brahma Engineering College Bhattacharjee, Sharmila; Govt. Degree College, Dharmanagar, Chemistry Daniliuc, Constantin; Universitaet Muenster, Organisch-Chemisches Institut Frontera, Antonio; Universitat de les Illes Balears Facultat de Ciencies, Química Lopato, Eric; Carnegie Mellon University Bernhard, Stefan; Carnegie Mellon University, Department of Chemistry

ARTICLE

Nickel(II) Complexes Based on Dithiolate-Polyamine Binary Ligand Systems: Crystal structures, Hirshfeld surface analysis, Theoretical Study, and Catalytic Activity Study in Photocatalytic Hydrogen Generation

Received 00th January 20xx,
Accepted 00th January 20xx

DOI: 10.1039/x0xx00000x

Suman Adhikari*[a], Tirtha Bhattacharjee[b], Sharmila Bhattacharjee[a], Constantin Gabriel Daniliuc[c], Antonio Frontera*[d], Eric M. Lopato[e], Stefan Bernhard[e]

To ascertain the influence of binary ligand systems [1,1-dicyanoethylene-2,2-dithiolate (*i-mnt*$^{-2}$) and polyamine {*tetraen* = tris(2-aminoethyl)amine, *tren* = diethylene triamine and *opda* = *o*-phenylenediamine}] on coordination modes of Ni(II) metal center and resulting supramolecular architectures, a series of nickel(II) thiolate complexes *[Ni(tetraen)(i-mnt)](DMSO)* (**1**), *[Ni$_2$(tren)$_2$(i-mnt)$_2$]* (**2**), and *[Ni$_2$(i-mnt)$_2$(opda)$_2$]$_n$* (**3**) have been synthesized in high yield in one step in water and structurally characterized by single crystal X-ray crystallography and spectroscopic techniques. X-ray diffraction studies disclose the diverse *i-mnt*$^{-2}$ coordination to Ni^{+2} center in active presence of polyamine ligands, forming slightly distorted octahedral geometry (NiN_4S_2) in **1**, square planar (NiS_4) and distorted octahedral geometry (NiN_6) in bimetallic co-crystallized aggregate of cationic *[Ni(tren)$_2$]$^{+2}$* and anionic *[Ni(i-mnt)$_2$]$^{-2}$* in **2**, and one dimensional (1D) polymeric chain along [*100*] axis in **3**, having consecutive square planar (NiS_4) and octahedral (NiN_6) coordination kernels. The N H···O, N H···S, N H···N, N H···S, N H···N, and N H···O type hydrogen bonds stabilize the supramolecular assemblies in **1**, **2,** and **3** respectively imparting interesting graph-set-motifs. The molecular Hirshfeld surface analyses (HS) and 2D fingerprint plots were utilized for decoding all types of non-covalent contacts in the crystal networks. Atomic HS analysis of Ni^{+2} centers reveal the significant Ni N metal-ligand interactions compared to Ni S interactions. We have also studied the unorthodox interactions observed in the solid state structures of **1**-**3** by QTAIM and NBO analysis. Moreover, all the complexes proved to be highly active water reduction co-catalysts (WRC) in a photo-catalytic hydrogen evolution process involving iridium photosensitizers, wherein **2** and **3** – having a square planar arrangement around nickel center(s) were found to be the most active, achieving 1000 and 1119 turn over numbers (TON) respectively.

Introduction

On account of their application as potentially building blocks in supramolecular materials with electrical conductivity, molecular magnetism, optoelectronic properties, and catalysis, metal complexes with sulphur rich ligands are currently of considerable interest.[1] Notably, binary ligands dithiolate based metal complexes have emerged as the most dynamic fields of chemistry due to their significance in the context of bioinorganic chemistry, versatile coordination chemistry, material properties, and industrial applications.[2] Nickel-thiolate complexes have attracted a great deal of attention due to their highly delocalized extending system and noteworthy building block for preparation of certain advanced materials with unusual catalytic and magnetic properties.[3] Given the facile redox states, potential for diverse ligation, and natural occurrence of Ni in [NiFe] hydrogenases[4], studying the activity of these unique Ni species as water reduction cocatalysts (WRCs) was a logical step. In particular, the discovery of the Nickel-thiolate complexes for photocatalytic and electrocatalytic hydrogen production in EtOH/H_2O solvent mixtures[5], strongly invigorated the investigation of Ni-thiolate complexes in the construction of supramolecular architectures having potential application in photo-catalytic hydrogen evolution.

Metal complexes incorporating sulphur-based multifunctional ligands such as 1,1-dicyanoethylene- 2,2-dithiolate (*i-mnt*$^{-2}$) and its geometric isomer 1,2-dicyanoethylene dithiolate (*mnt*$^{-2}$) are remarkable for their wide-ranging π-electron delocalization, reversible redox behaviour and had been a subject of notable consideration.[6] The ligand *i-mnt*$^{-2}$ represents an especially intriguing multifunctional building blocks owing to the presence of two anionic sulphur atoms and two nitrogen atoms of cyanide groups capable of binding to metal ions, for both complexation and non-

[a] *Department of Chemistry, Govt. Degree College, Dharmanagar, Tripura (N)-799253, India*
[b] *Department of Chemistry, Bineswar Brahma Engineering College, Kokrajhar-783370, Assam, India*
[c] *Organisch-Chemisches Institut, Westfälische Wilhelms-Universität Münster, Corrensstraße 40, D-48149, Münster, Germany,*
[d] *Department de Quimica, Universitat de les Illes Balears, Crta. de Valldemossa km 7.5, 07122 Palma de Mallorca (Baleares), Spain*
[e] *eDepartment of Chemistry, Carnegie Mellon University, 4400 Fifth Avenue, Pittsburgh, Pennsylvania 15213, United States.*
† Footnotes relating to the title and/or authors should appear here.
Electronic Supplementary Information (ESI) available: [details of any supplementary information available should be included here]. See DOI: 10.1039/x0xx00000x

covalent interactions and thus can be utilized to develop metal organic frameworks with unique properties.[7] The blend of coordination features and non-covalent interactions feasibilities ensure rich metallo-supramolecular chemistry/coordination frameworks of *i-mnt*$^{-2}$ based complexes. Regarding the above considerations, *i-mnt*$^{-2}$ with bridging capacity and multiple binding sites is a good choice for the formation of supramolecular structures in combination with other N-donor polyamine ligands. Although extensive effort has been devoted to the problem of design and synthesis of Nickel-thiolate binary ligand complexes, the number of accessible frameworks, particularly with crystallographic evidence, stays limited and the physical property determinants remain recondite. The above aspects increased our enthusiasm for exploring the chemistry of Nickel-thiolate complexes. The amalgamation of the electronic, structural, and binding properties of *i-mnt*$^{-2}$ and appropriate N-donor polyamine ligands enables cooperative electronic materials with potential applications.

In this article, we report the use of simple binary ligand based complexes assembled from nickel salt with *i-mnt*$^{-2}$ and polyamines in one step in water as the highly active water reduction catalysts. We also employed our characterization toolbox including classical structure description along with HS analysis and DFT calculations of interaction energies in order to quantify energetic contributions of different non-covalent contacts into these structural features. Moreover, the structural descriptions of synthesized complexes were also substantiated with HS analysis and DFT calculations. Since, the numerous non-covalent interactions present in the supramolecular system offer the prospect towards a deeper understanding of the complicated processes regulating the supramolecular design and the selectivity/reactivity of chemical transformations is regulated by these weak non-covalent forces.[8] Catalytic experiments herein were performed using iridium photosensitizers. Cationic iridium (III) complexes have demonstrated significant ability in photocatalytic reactions[9], namely water reduction[10], due to their long-live, charge separated triplet excited state induced by spin-orbit coupling from the iridium center.[11] There is a history of highly active mononuclear Ni WRCs including similar bonding moieties, namely, thiolate[12] and tetraaza-macrocycles.[13] Binuclear and polynuclear Ni complexes have also seen significant work in photocatalytic water reduction.[14]

Experimental

Materials and physical measurements

All chemicals were reagent grade obtained from commercial sources and used without purification. The solvents were purified by standard procedures. The 1,1-dicyano-2,2-ethylenedithiolate dipotassium salt (K_2*i-mnt*) was synthesized according to procedure reported previously.[15] Infrared spectra were measured on a Perkin-Elmer FT-IR spectrometer with KBr pellets in the range of 4000–500 cm^{-1}. NMR spectra were recorded on Bruker Advance II (400MHz) spectrometer using the residual protic solvent resonance as the internal standard and chemical shifts were expressed in ppm. Elemental analysis was carried out in PerkinElmer 2500 series II elemental analyzer. Cyclic voltammetry was performed using a three- electrode system on a CH-Instruments Electrochemical Analyzer 600C potentiostat. All scans were performed at a rate of 0.1 V/s with negative scan polarity. UV-vis spectra were recorded on a Perkin Elmer model Lambda 25.

Synthesis of the metal complexes

Complexes were synthesized in one step in water and afforded high yields. A schematic representation of the synthetic procedure is shown via Scheme 1.

A solution of $NiCl_2{}^*6H_2O$ (1.27 mmol) in 20 mL distilled water was added slowly to ligand *tetraen* (3.81 mmol) dissolved in 20 mL water, with constant stirring at room temperature, and stirring continued for 1 h. K_2*i-mnt*·H_2O (1.27 mmol) dissolved in 20 mL water was added with stirring to this reaction mixture, resulting immediate formation of precipitate and stirring was continued for further 1 h. The precipitate obtained was filtered, washed several times with distilled water and ether, and dried in vacuo over fused $CaCl_2$. Single crystals of **1** were grown from saturated solution of Dimethyl Sulphoxide (*DMSO*). IR, ^{1}H NMR and UV-Vis data are given in the experimental section and in the ESI†. For complex **1** and **2** NMR spectra is dominated by the paramagnetic properties of the complexes and no significant peaks were detected.

Complex 1: Yield: 81%, FTIR (ν cm^{-1}, KBr): 3297-3251 {ν(N-H) asymmetric and symmetric stretching modes}, 2201 (νCN stretching), 1582 (νN-H bending scissoring vibration), 1366-1316 {ν(C=C) absorption band}, 985 {ν(=CS_2) group, 887 {ν(C- S). UV-vis. (4% DMSO in $CHCl_3$, λ_{max}/nm): 317, 356, 546. Anal. Calc. for $C_{12}H_{24}N_6NiOS_3$: C, 34.05; H, 5.72; N, 19.86 %. Found: C, 34.03; H, 5.69; N, 9.83%.

The synthetic procedures for **2** and **3** were similar to that of 1, except that ligands *tren* and *opda* were used instead of ligand *tetraen*. Single crystals of **2** and **3** were grown from saturated solution of *N,N*-dimethyl formamide (*DMF*).

Complex 2: Yield: 84%, FTIR (ν cm^{-1}, KBr): 3336-3260 {ν(N-H) asymmetric and symmetric stretching modes}, 2203 (νCN stretching), 1584 (νN-H bending scissoring vibration), 1401-1380 {ν(C=C) absorption band}, 964 {ν(=CS_2) group, 893 {ν(C- S) band}. UV-vis. (4% DMSO in $CHCl_3$, λ_{max}/nm): 318, 414, 603. Anal. Calc. for $C_{16}H_{26}N_{10}Ni_2S_4$: C, 31.81; H, 4.34; N, 23.19 %. Found: C, 31.83; H, 4.33; N, 23.17%.

Complex 3: Yield: 82%, ^{1}H NMR (400 MHz, DMSO-d_6, δ in ppm): 6.40 (d, 4H, Ar-H), 4.30 (brs, 4H, -NH_2). FTIR (ν cm^{-1}, KBr): 3552-3360 {ν(N-H) asymmetric and symmetric stretching modes}, 2203 (νCN stretching), 1569 (νN-H bending scissoring vibration), 1368 {ν(C=C) absorption band}, 948 {ν(=CS_2) group, 899 {ν(C-S) band}. UV-vis. (4% DMSO in $CHCl_3$, λ_{max}/nm): 317, 371, 434. Anal. Calc. for $C_{26}H_{30}N_{10}Ni_2O_2S_4$: C, 41.08; H, 3.98; N, 18.42 %. Found: C, 41.06; H, 3.99; N, 18.44%.

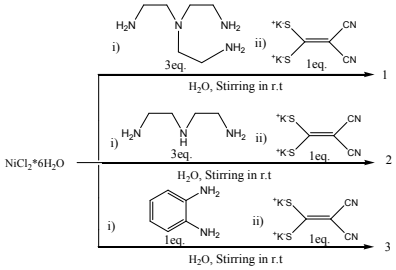

Scheme 1. Schematic representation of the synthetic procedure.

X-ray crystallography data collection and structure refinement

For compounds **1**, **2**, and **3** data sets were collected with a Nonius Kappa CCD diffractometer. Programs used: data collection, COLLECT[16]; data reduction Denzo-SMN[17]; absorption correction, Denzo[18]; structure solution *SHELXT-2015*[19]; structure refinement *SHELXL-2015*[20]. R-values are given for observed reflections, and wR^2 values are given for all reflections. In **1**, the *DMSO* is disordered over two positions, and to improve refinement stability, several restraints (SADI, SAME, ISOR and SIMU) were used. A summary of crystallographic data and structure refinement details for **1**-**3** are mentioned in **Table 1**. All bond lengths, bond angles and torsion angles of complexes **1**-**3** are depicted in **Table S1-S3**.

Hirshfeld Surface Analysis

The 3D Hirshfeld surfaces (HS) and 2D fingerprint plots[21-24] for **1**-**3** were obtained by using Crystal Explorer 17.5 program package.[25] The 3D Hirshfeld surfaces were mapped over d_{norm}, shape index and curvedness[22], where each point on the surface reveals information about *d*i, *d*e, and *vdW*; surface point to nearest interior nucleus distance, surface point to nearest exterior nucleus distance and van der Waals radii of atoms respectively. The d_{norm}[23] parameter is defined as:

$$d_{norm} = \frac{(d_i - r_i^{vdW})}{r_i^{vdW}} + \frac{(d_e - r_e^{vdW})}{r_e^{vdW}}$$

The red, white, and blue regions on HSs expounded as shorter contacts (d_{norm} -ve), contacts in the range of van der Waals separation (d_{norm} = 0) and longer contacts (d_{norm} +ve) respectively.

.

Theoretical methods

The calculation reported herein were carried out using Gaussian-09[26] at the B3LYP/def2-TZVP level of theory. Bader's quantum theory of "Atoms in molecules" QTAIM has been used to study the interactions discussed herein by means of the AIMall calculation package.[27] The calculations for the wavefunction analysis as well as NBO 3.0 (Natural Bonding Orbital) calculations were carried out at the same level of theory.

Photocatalytic Hydrogen Evolution

Testing of compounds **1**, **2**, and **3** as water reduction cocatalysts (WRCs) for photocatalytic reactions were performed in a unique parallelized photoreactor.[28] The well-studied [Ir(Fmppy)2dtbbpy]PF6 (where Fmppy = 4'-fluoro-2-phenyl-5-methylpyridine, dtbbpy = 4,4'-di-tert-butyl-2,2'-bipyridine)[29] was utilized as a photosensitizer (PS) in this system. 1 mL shell vials were populated with 600 microliters of PS and WRC solutions in DMSO (J.T. Baker JT 9224), and 150 microliters of a 30% (w/w) solution of triethanolamine (TEOA) (Alfa Aesar L04486) in water, as a sacrificial electron donor. Reactions consisted of a range of PS concentration from 0 through 0.75 mM, WRC concentrations ranging from 0 to 0.1 mM, and were illuminated using water cooled 100 W blue light-emitting diodes (LEDs) (440 +/- 10 nm) for 1000 minutes, monitored every 10 minutes by photography of a commercially available colorimetric hydrogen sensitive tape (DetecTape Hydrogen Detection Tape – Midsun Specialty Products, Item DT-H210015-PF4). These images were processed through a Wolfram Mathematica Script to determine the quantity of hydrogen produced through time.

Results

Recapitulation of crystal structures

[Ni(tetraen)(i-mnt)](DMSO):

Single crystal XRD analysis revealed that the complex *[Ni(tetraen)(i-mnt)](DMSO)* (**1**) crystallises in the monoclinic crystal system with space group $P2_1/n$, and the asymmetric unit composed of one Ni(II) ion, *tetraen*, *i-mnt*$^{-2}$, and one solvent molecule (*DMSO*) disordered over two positions as shown in **Figure 1**. In **1,** Ni^{+2} is hexa-coordinated with NiN_4S_2 coordination environment and exhibits distorted octahedral geometry where the Ni(II) metal center coordinated to four amino N-atoms (N3, N4, N5, N6) of archetypal tripodal flexible chelate *tetraen* in a trichelated fashion and *i-mnt*$^{-2}$ chelated to Ni^{+2} through two thiolate S-atoms (S1,S2) providing overall neutrality to coordination sphere while two cyano ends of *i-mnt*$^{-2}$ remain free. In the slightly distorted octahedral geometry of **1**; S1,S2,N4,N5 occupy the corners of basal plane and axial sites are occupied by N3, N6 atoms where Ni^{+2} resides at the centre of basal plane and axial Ni N bonds slightly tilt towards *tetraen* moiety. The distortion around Ni(II) center is evident from trans angles $162.9(1)^0$ [N3 Ni1 N6] and $174.0(1)^0$ [N5 Ni1 S2] which might be due to the intra and intermolecular interactions of thiolate ends (*i-mnt*$^{-2}$) and the inherent tendency of tetradentate *tetraen* to offer trigonal bipyramidal coordination cap to any metal center cannot be ruled out.[30-33] A similar attempt was made with Zn(II) salt, *tetraen*, and *i-mnt*$^{-2}$ that yielded trigonal bipyramidal geometry[34] instead of octahedral. The solvent molecule, *DMSO* offers stability to crystal structure by forming intermolecular hydrogen bonds with amino N H donors. Summary of all the intermolecular interactions are depicted in **Table S4**. The close proximity of cyano end (*i-mnt*$^{-2}$) and sulfoxide S-atom of DMSO opens up the possibility of σ-hole chalcogen bonding interaction. The N H···O, N H···S type H-bonds and van der Waals interactions are believed to be responsible for crystal stability. These H-bond connectors link the molecules forming a 3D supra-molecular stacking assembly along *ab* plane (**Figure S10).** We can visualize a segment of the stacked assembly as 3D right handed helical arrangement along *ac* plane imagining axis of the helix passing through Ni(II) atoms of each asymmetric unit (**Figure 2**). These repeating hydrogen bonds throughout the crystal structure generate finite chain, infinite chain, and ring geometrical arrays of graph-set-motifs D, C(6), C(4), $R_3^2(8)$, $R_2^1(6)$, and $R_4^2(10)$ respectively.

Table 1 Crystal Data and Structure Refinement Summary for **1**-**3.**

	1	**2**	**3**
Empirical formula	$C_{12}H_{24}N_6NiOS_3$	$C_{16}H_{26}N_{10}Ni_2S_4$	$C_{26}H_{30}N_{10}Ni_2O_2S_4$
Formula weight	423.26	604.13	760.26
Temperature /K	173(2)	173(2)	173(2)
Crystal system	monoclinic	monoclinic	monoclinic
Space group	$P2_1/n$	$C2/c$	$C2/m$
a /Å	8.3663(2)	16.3199(6)	18.658(4)
b /Å	14.6831(3)	9.1021(3)	7.2167(14)
c /Å	15.5009(4)	18.1332(7)	14.534(3)
α /^{0}	90	90	90
β /^{0}	99.3820(10)	114.143(3)	120.13(3)
γ /^{0}	90	90	90
V /A^3	1878.71(8)	2457.99(16)	1692.697)
Z	4	4	2
ρ_{cal} /gcm^{-3}	1.496	1.633	1.492
μ /mm^{-1}	1.377	1.898	1.400
F(000)	888	1248	784
Crystal size /mm^3	0.020x0.060x0.080	0.020x0.030x0.060	0.020x0.060x0.090
θ range /^{0}	4.08 28.20	4.37 28.17	4.21 28.20
Reflections collected	8391	5608	3885
Independent reflections	4553 [R_{int} = 0.0312]	2999 [R_{int} = 0.0512]	2226 [R_{int} = 0.0338]
Absorption correction	multi-scan	multi-scan	multi-scan
Max and min transmission	0.973 and 0.898	0.9630 and 0.8950	0.9730 and 0.8840
Data/restraints/parameters	4553/64/257	2999/0/167	2226/67/150
Goodness-of-fit on F^2	1.053	1.025	1.046
Final R indices [$I > 2\sigma(I)$]	R_1 = 0.0383, wR_2 = 0.0916	R_1 =0.0495 , wR_2 =0.1053	R_1 =0.0464 , wR_2 =0.1177
Final R indices [all data]	R_1 = 0.0463, wR_2 = 0.0963	R_1 =0.0673 , wR_2 = 0.1148	R_1 =0.0564 , wR_2 = 0.1261
Largest difference in peak and hole /e A^3	0.403 and -0.729	0.438 and -0.43	0.626 and -0.439

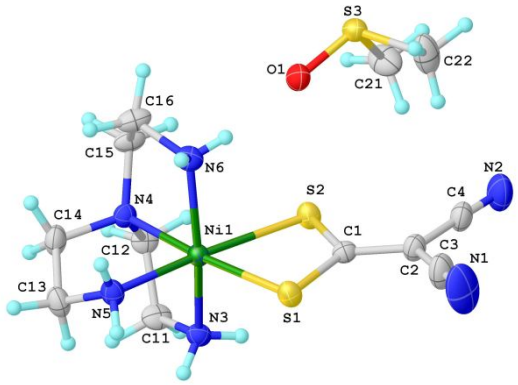

Figure 1. Molecular structure of **1**, showing the atom labelling scheme with 50% probability ellipsoids.

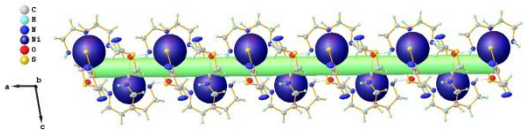

Figure 2. Crystal packing arrangement as 3D right handed helix along *ac* plane.

[$Ni_2(tren)_2(i\text{-}mnt)_2$]:

The complex *[$Ni_2(tren)_2(i\text{-}mnt)_2$]* (**2**) crystallises in monoclinic crystal system, space group *C*2/*c*, with two half Ni^{+2} ions, one *tren*, and one *i-mnt*$^{-2}$ in the asymmetric unit. The bimetallic chelate **2** exists as co-crystallized aggregate of cationic *[Ni(tren)$_2$]$^{+2}$* and anionic *[Ni(i-mnt)$_2$]$^{-2}$* (**Figure 3**). The two Ni^{+2} ions present hexa-coordinated and tetra-coordinated environments and exhibit octahedral and square planar geometry respectively. In NiS_4, four thiolate S-atoms (S1,S2,$S1^{ii}$,$S2^{ii}$) [(ii) -x+1, -y+1, -z] coordinated to Ni^{+2} in a trans bischelated fashion and occupy four corners of the square planar geometry. The Okuniewski parameter[35] τ'_4=0 [$\tau'_4 = \frac{\beta-\alpha}{360^0-\theta} + \frac{180^0-\beta}{180^0-\theta}$, β>α and θ = $\cos^{-1}(-1/3)$~109.5^0, where τ_4'=0 means square planar, τ_4'=1 means tetrahedral geometry] confirms square planar coordination kernel (β = 180.0° [S2 Ni1 $S2^{ii}$], α = 180.0° [S1 Ni1 $S1^{ii}$]).

In NiN_6 coordination environment, six amino N-atoms (N3,N4,N5,$N3^i$,$N4^i$,$N5^i$) [(i) -x+1, y, -z+½] of *tren* chelated to Ni^{+2} in a slightly distorted octahedral fashion where N3,$N3^i$,N4,$N4^i$ occupy corners of basal plane, terminal amino N-atoms (N5,$N5^i$) occupy trans axial sites and deviation of Ni(II) metal center from centroid of basal plane is 0.055(3) Å. The trans angles 171.5(1)° [N3 Ni2 $N4^i$] and 168.5(2)° [N5 Ni2 $N5^i$] and bite angles varying in the range

82.7(1)° to 102.8(2)° justify distortion in octahedral geometry. The normal angle, twist angle, and fold angle between square planar plane (S1,S2,S1^{ii},S2^{ii}) and octahedral basal plane (N3,N3^{i},N4,N4^{i}) are found to be 58.6(1)°, 55.4(1)°, 49.5(1)° respectively. The Ni···Ni distances 5.592(1) Å [Ni1···N2], 9.102(1) Å [Ni1···Ni1] and 16.320(1) Å [Ni2···Ni2] [more than the sum of van der Waals radii of two Ni(II) atoms] confirm the absence of Ni(II)···Ni(II) metallophilic interaction.[36] Summary of all the hydrogen bond parameters are listed in **Table S4**. The N4 H4···S1 intramolecular hydrogen bond is the only connector between NiS_4 and NiN_6 coordination spheres that forms finite chain geometry of D type graph-set-motif and the N H···N type intermolecular H-bonds form infinite chain geometry of C(8) type graph-set-motif. Undoubtedly, N H···S and N H···N H-bonds (**Figure S11**) along with van der Waals interactions contribute immensely in stabilizing the crystal structure. These connectors interconnect molecules in **2** leading to the formation of 3D supramolecular zic-zac stacked chains along *bc* plane as shown in **Figure 4**.

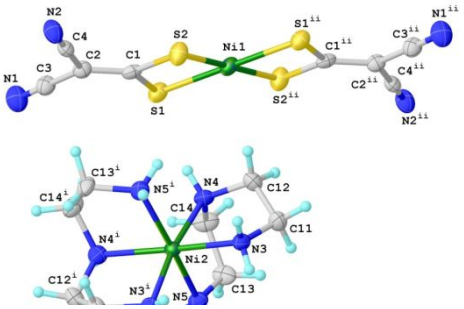

Figure 3. Molecular structure of *[Ni$_2$(tren)$_2$(i-mnt)$_2$]* showing the atom labelling scheme with 50% probability ellipsoids. (symmetry codes: (i) -x+1, y, -z+½; (ii) -x+1, -y+1, -z)

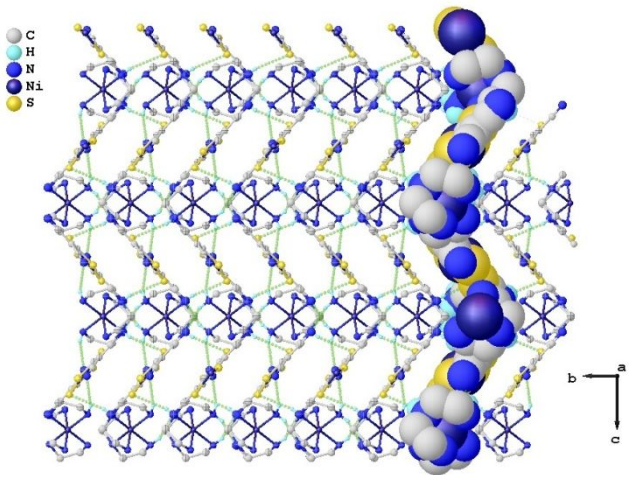

Figure 4. Projection of 3D supramolecular stacked chains along *bc* plane for **2** (Hydrogen bonds as dotted lines).

[Ni$_2$(i-mnt)$_2$(opda)$_2$]$_n$:

The complex *[Ni$_2$(i-mnt)$_2$(opda)$_2$]$_n$* (**3**) crystallizes in the monoclinic crystal system, space group *C*2/*m*, and the asymmetric unit consists of two half Ni(II) ion, a complete *i-mnt*$^{-2}$ ligand, half *opda*, and one disordered over two positions solvent molecule (*DMF*). It is a binuclear Ni(II) polymeric complex having two discrete NiS_4 and NiN_6 coordination spheres linked *via i-mnt*$^{-2}$ (**Figure 5**). The S_4 donor set comprises of four thiolate S-atoms (S1,S2,S1^{i},S2^{i}) [(i) -x+2, -y-2, -z+1] of two *i-mnt*$^{-2}$ that chelated to Ni^{+2} in a bischelated fashion generating square planar geometry. The existence of perfect square planar kernel is confirmed from Okuniewski parameter[35] τ'_4=0 (β = 180.0 [S2 Ni1 S2^{i}], α = 180.0° [S1 Ni1 S1^{i}]). While in NiN_6, Ni^{+2} is coordinated by two amino N-atoms (N3,N3^{ii},N3^{iii},N3^{iv}) [(ii) -x+2, -y-2, -z; (iii) x, -y-2, z; (iv) -x+2, y, -z.] of two *opda* in bischelated fashion and two cyano N-atoms (N1, N1^{iii}) of two *i-mnt*$^{-2}$. The *i-mnt*$^{-2}$ in presence of *opda*, connects two nearby Ni^{+2} ions in a tridentate fashion through thiolate and cyano terminals, thereby forming a one dimensional (1D) infinite polymeric chain of consecutive NiS_4 and NiN_6 kernels that propagates along [100] axis (**Figure 6**). In the octahedral geometry of NiN_6, N3,N3^{ii},N3^{iii},N3^{iv} (*opda*) occupy corners of basal plane; N1, N1^{iii} (*i-mnt*$^{-2}$) occupy trans axial sites perpendicular to basal plane and metal center resides at the centroid of basal plane. Small distortion in octahedral geometry is observed due to little variation in bite angles ranging from 83.2(1)° to 96.8(1)°. All the Ni2 N [2.088(2) Å] bond lengths in basal plane are found to be similar and the same trend is followed for apical Ni2 N bonds [2.110(3) Å]. The twist angle 90.0(2)° justifying perpendicular arrangement of square planar and octahedral basal plane contrary to 2 and large Ni1···N2 [7.267(2) Å] distance discard the possibility of metallophilic interaction.[36] Square planar geometry for NiS_4 in **2** and **3** are almost identical, on the contrary octahedral kernels are quite different due to the influence of secondary ligand (*opda*). The distance between S1 atom of *i-mnt*$^{-2}$ and centroid of phenyl ring (*opda*) [3.809(3) Å] exceeds the sum of van der Waals radii (3.5 Å),[37] suggesting absence of any anion···π interaction.

The summary of all hydrogen bond parameters are listed in **Table S4**. The neutral *DMF* solvent molecules link the parallel 1D polymeric chains via N3 H3A···O1 hydrogen bonds forming 2D supramolecular chain like arrangement along *ab* plane assuming that *DMF* molecules reside at the crystal voids and NiS_4 kernels (*sp*) perpendicular to the chain (**Figure 7**). These N H···O connectors among two *DMF* and two NiN_6 moieties in parallel polymeric chain, generate twelve membered ring like geometrical array of $R_4^2(12)$ graph-set-motif. These 2D packed chains are further interconnected *via* N3 H3B···N2 hydrogen bonds between *opda* N3 H3B donors and free cyano end acceptors (N2) of *i-mnt*$^{-2}$, which extends in three dimension leading to the formation of 3D supramolecular circular ribbon like stacked assembly as shown in **Figure S12**. Formation of twenty-eight membered ring like structure due to N3 H3B···N2 connector can be assigned as $C(14)R_2^2(28)$ type graph-set-motif.

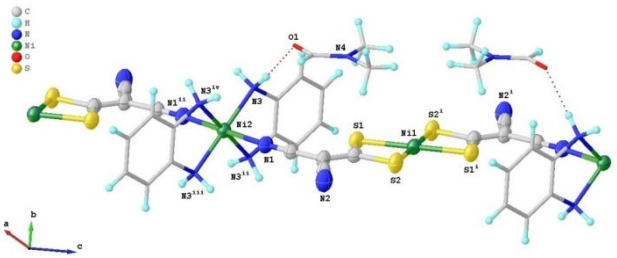

Figure 5. Perspective view polymeric segment showing coordination environment around Ni(II) metal center.[symmetry code (i) -x+2, -y-2, -z+1; (ii) -x+2, -y-2, -z; (iii) x, -y-2, z; (iv) -x+2, y, -z; (v) x+½, y+½, z.].

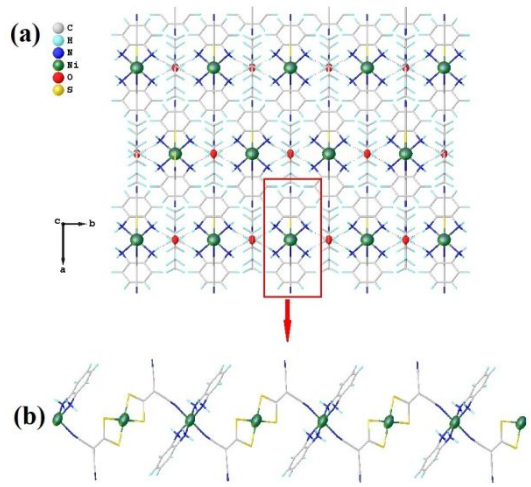

Figure 6. (a) View of the 3D supramolecular assembly. (b) Segment of polymeric chain.

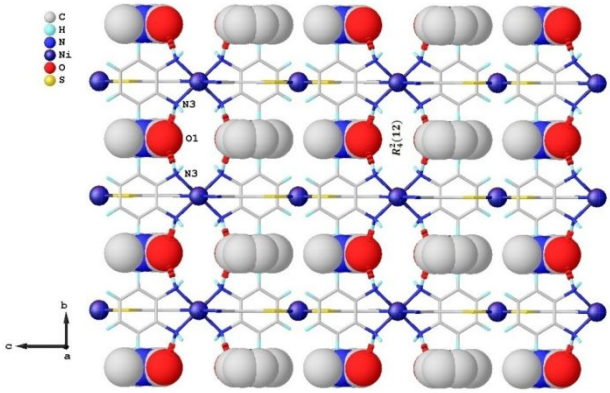

Figure 7. View of the 2D supramolecular chain assembly along *bc* plane. The N3 H3A···O1 hydrogen bonds shown as red dotted lines.

Hirshfeld surface analysis

The Hirshfeld surface (HS)[21,22] and associated two dimensional (2D) fingerprint (FP) plots are exceedingly useful tools that offer unambiguous analysis of multicomponent crystal structures,[38] revealing detailed immediate environment of a molecule and quantify all possible non-covalent intermolecular interactions formed by the molecule in question thereby permitting systematic comparison of related crystal structures.[39-41] The X-ray diffraction study reveals fascinating coexistance of independent cationic (*oc*) and anionic (*sp*) species as cocrystalline aggregates in **2** and 1D polymeric chain in **3**. These versatility of binary ligand-based nickel complexes tempt us to explore further non-covalent interactions by HSs study. The HS mapped seperately for the anionic $[Ni(i\text{-}mnt)_2]^{-2}$ [**2A**] and cationic $[Ni(tren)_2]^{+2}$ [**2B**] species in **2** while for **3**, square planar [**3A**] and octahedral [**3B**] segment in the repeat polymeric unit $[Ni_2(i\text{-}mnt)_2(opda)_2]$ are studied seperately. The 3D HS mapped with d_{norm} and 2D FP plots for **1**-**3** are depicted in **Figures 8, 9.** The standard (high) surface resolution criteria was chosen and surface transparency option enabled for clear visualization and identification of interactions through the mapped surfaces. The requisite quantitative information regarding molecular volume (V_H), surface area (A_H), globularity (G), and asphericity (Ω) are mentioned in **Table 2**. The octahedral **1**, **2B**, and **3B** have higher Hirshfeld volumes (V_H) and surface areas (A_H) expect **2B** due to compact shaped. All the asymmetric units have well defined 3D structured molecular surface as globularity[42] values are less than one and **2B** has the most convex HS. The asphericity[43] data clearly showing greater anisotropy properties of **2A** and **3A** (**Table 2**).

The intense red depressions on d_{norm} HS around cyano end of $i\text{-}mnt^{-2}$ (**1**, **2A**, **3A**), amino end of *tetraen* (**2B**) and *opda* (**3B**) indicating strong N···H/H···N intermolecular interactions arising from N H···N and C H···N type hydrogen bonds (**Table S4)** and dull red spots appear around thiolate end of $i\text{-}mnt^{-2}$ (**1**, **2A**) denote moderate S···H contacts due to N H···S hydrogen bonds. On the contrary weak S···H contacts appear as white spots in **3A**. The deep red depressions in **1** and **3B** observed for strong H···O contacts assigned to $N_{coordinated\ tetraen}$ H···O_{DMSO} and $N_{coordinated\ opda}$ H···O_{DMF} hydrogen bonds respectively. The remaining faded red regions and white areas on HS originate from weak C···H/H···C and H···H contacts respectively while blue areas indicate absence of any interaction. The HS mapped on shape index and curvedness are devoid of any red or blue triangle (bow-tie pattern) (**Figure S13**) and no flat surface patches nullifying the possibility of π···π and C H···π interactions.

The two dimensional (2D) fingerprint plots for **1**-**3** based on *d*i versus *d*e in the translated range, appeared as distinct upper donor and lower acceptor spikes, representing N···H/H···N contacts around 2.2 Å $<d_e+d_i<$ 2.8 Å (**1**, **2B**, **3B**), S···H/H···S contacts around 2.4 Å $<d_e+d_i<$ 3.2 Å (**Figure 9 and Figures S14, S15**) and C···H/H···C contacts around d_e+d_i ~ 2.8 Å. The sharp blue spikes appeared around d_e+d_i ~ 2 Å, denote strong H···O contacts (**1**, **3B**). The H···H contacts that bestows crystalline lattice strength, appeared as scattered points, spreading up to $d_i = d_e = 2.5$ Å for **1,** 2.1 Å $< d_i = d_e <$ 2.6 Å for **2B**, and $d_i = d_e = 2.4$ Å for **3B**. From the 2D FP plots it is obvious that apart from H···H and other minor contacts, hydrogen bond interactions account for more than half (**1**, 61.7%; **2A**, 86%; **2B**, 72%; **3A**, 86.1%; **3B**, 65.5%) which play leading role in supramolecular crystal packing. In **2A**, the predominant S···H, and N···H contacts (34.0% and 35.4%) arise from strong N H···N and N H···S hydrogen bonds (**Table S4**) between **2B** and **2A**. The small but substantial Ni···H contact (3.5%) explaining the possibility of C H···Ni interaction (2.966 Å) between anionic (**2A**) and cationic (**2B**) fragments (**Figure S16**). The H···N, H···S, and H···C contacts are found to be less in octahedral complexes (**1**, **2B**, **3B**) compared to square planar ones (**2A**, **3A**). The **3A**, due to 1D polymer formation *via* cyano end of $i\text{-}mnt^{-2}$, experiences lower N···H interaction (32.4%) compared to non-polymeric **2A**, in fact, the later has maximum N···H and S···H interactions compared to the rest. The comparative distribution of non-covalent interactions (percentage scale) are shown as 3D stacked bar diagram in **Figure 10.**

To evaluate the impact of diverse ligand coordination to metal center in **1**-**3**, we have also performed HS analysis[44,45] for nickel center. In contrast to molecular HS, slight change of coordination direction or nature of ligand impact HS of metal center with significant depressions which in turn changes HS properties like volume, globularity etc.[21-24] It is evident from the comparatively

high volume, surface area, and globularity for octahedral complexes (**1**, **2B**, **3B**) compared to square planar ones (**2A** and **3A**) inferring further deviation of surface area from that of a sphere for the later (**Table 3)**. Moreover, huge difference in asphericity (Ω) indicates much higher anisotropy in square planar complexes compared to octahedral ones evince the fact that metal complexes (**2A** and **3A**) having longer coordination bonds, exhibit higher anisotropic metal surface. Larger volume and surface areas of square planar complexes also impacted on 2D FP plots revealing higher *d*i, *d*e limiting values. The Ni–N coordination bonds appeared as circular bright-red spots perpendicular to the Ni–N bond direction on HS mapped over d_{norm} (**Figure 11)**. The Ni–N bond strength is evident from the rectangular orange spots and green flat regions on HS mapped with shape-index (S) and over curvature (C), respectively (**Figure S13**). The slight differences in Ni S bond lengths are evident from the irregular orange patches surrounded by yellow regions on HS mapped over shape-index (**Figure S13**). Sulphur atoms coordinated to Ni-centers through the regions outside the orange patches on HS indicating deviations of the Ni–S bonds from the normal of the surfaces. In the 2D FP plots, the prominent long red spikes at *d*e + *d*i ≈ 2.1 Å indicate Ni–N bonds for **1** (lower spike), **2B** and **3B**; whereas the red spikes at *d*e + *d*i< 2.4 Å indicate Ni–S bonds for **1** (upper spike), **2A** and **3A** (**Figure 12**). The 2D FP shows contribution of Ni N and Ni S co-ordinations are in the order of **3B** (78.3%) > **2B** (73.7%) > **1** (53.6%) and **3A** (59.8%) > **2A** (56.3%) > **1** (24.7%) respectively. Furthermore, the Ni···H contacts in square planar complexes **3A** (40.2%) and **2A** (43.8%) have higher contribution, compared to octahedral complexes **1** (21.6%), **2B** (26.3%), **3B** (21.7%).

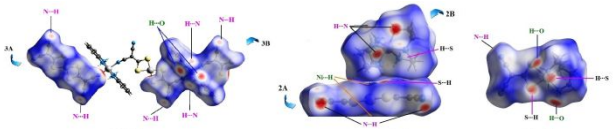

Figure 8. View of Hirshfeld surfaces mapped over d_{norm}.

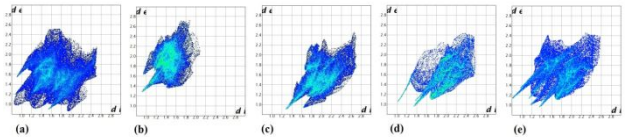

Figure 9. 2D fingerprint plots for (a) **1** (b) **2B** (c) **2A** (d) **3A** (e) **3B**.

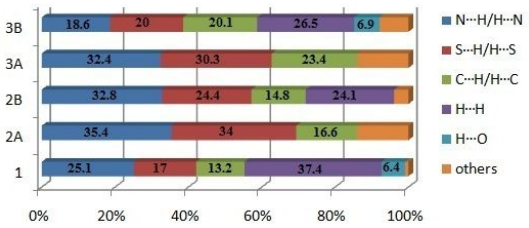

Figure 10. Stacked bar diagram illustrating the relative distribution of interactions from HS analysis for **1**-**3**.

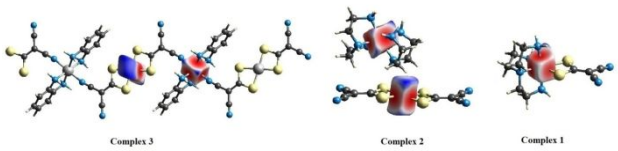

Figure 11. View of Hirshfeld surfaces for nickel center in **1**-**3** mapped over d_{norm}.

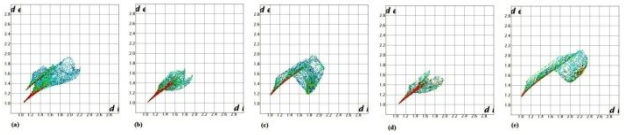

Figure 12. View of 2D finger print plots for nickel center in (a) **1** (b) **2B** (c) **2A** (d) **3B** (e) **3A**.

Table 2. Quantitative data from Hirshfeld surface of **1**-**3**.

Complex	V_H (Å^3)	A_H (Å^2)	G	Ω
1	360.72	304.19	0.806	0.120
2A	299.58	293.38	0.738	0.333
2B	302.18	259.32	0.840	0.033
3A	295.56	283.60	0.757	0.353
3B	569.44	486.80	0.682	0.150

Table 3. Quantitative data from Hirshfeld surface of Ni-metal centers in **1**-**3**.

Ni^{+2} in	V_H (Å^3)	A_H (Å^2)	G	Ω
1	11.09	28.12	0.855	0.025
2A	13.50	31.71	0.864	0.099
2B	10.82	28.00	0.854	0.016
3A	16.71	37.47	0.844	0.188
3B	10.63	28.42	0.823	0.019

Theoretical study of complexes

Experimentally, three new Ni(II) complexes have been synthesized and X-ray characterized. The theoretical analysis is devoted to the study of some unorthodox interactions observed in the solid state of these compounds using two different computational tools: (i) the QTAIM analysis to confirm existence and characterize the interactions and (ii) the NBO analysis to investigate if orbital donor-acceptor interactions are energetically relevant.

In compound **1,** we have analyzed one of the interaction modes of the complex with the co-crystalized *DMSO* solvent molecule. In **Figure 13a** we show a partial view of the solid state structure of **1** and the *DMSO* where it can be observed that the N atom of the *i-mnt*$^{-2}$ co-ligand points to the S-atom of the *DMSO* opposite to the S–CH_3 bond. This is typical of σ-hole chalcogen bonding interactions. We have used the QTAIM to confirm the existence of this interaction by examining the distribution of bond critical points (CPs) and bond paths of the dimer, as shown in **Figure 13b**. The chalcogen bond is characterized by the existence of a bond CP (green sphere) and bond path interconnecting the N and S atoms, thus confirming the interaction. Moreover, an additional bond CP and bond path connects the N atom to one H-atom of the methyl group, thus revealing the formation of an H-bond. The density at the bond CP that characterizes the chalcogen bond is larger than that at the CP that characterizes the H-bond, thus suggesting that the chalcogen bond is energetically more favorable. We also performed the natural bond orbital analysis (NBO)[46] of this complex. We have focused our attention on the second order perturbation analysis since it is very convenient for the evaluation of donor–acceptor interactions from an orbital point of view.[47] We have found two donor-acceptor orbital interactions involving the N-atom of the dianionic ligand as donor and the *DMSO* molecule as acceptor. As typically in chalcogen bonds, there is an electron donation from the LP orbital of the N atom to the antibonding

σ*(S–C) orbital with a concomitant stabilization energy of $E^{(2)}$ = 3.01 kJ/mol. This energy is modest due to the small polarization of the S–C bond. For the H-bond, we have also found an electron donation from the LP orbital of the N atom to the antibonding σ*(C–H) with a concomitant stabilization energy of $E^{(2)}$ = 0.33 kJ/mol. This result agrees well with the electron charge density at the bond CP that is larger for the chalcogen bond.

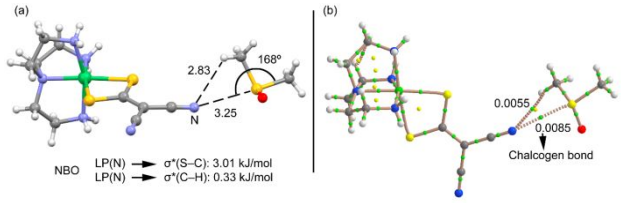

Figure 13. (a) X-ray fragment with indication of the combination of chalcogen and hydrogen bonds. Distances in Å. The results from the NBO calculations are also indicated. (b) Distribution of bond and ring CPs (green and yellow spheres, respectively) for the dimer. The values of ρ(r) at the bond CPs are given in a.u.

In compound **2**, we have analyzed the C–H···Ni(II) interactions that are established between the anionic and cationic fragments in the crystal structure, as indicated in **Figure 14a**. The short Ni···H distance indicates that in addition to the electrostatic attraction between the counter-ions, the final geometry of the assembly could be modulated by this interaction. We wonder if it is an agostic interaction where the C–H sigma bond acts as electron donor to the empty d orbital of Ni(II) or if it is a hydrogen bonding interaction where the dianionic moiety acts as electron donor using a filled d orbital of Ni(II) (unconventional H-bond). The QTAIM distribution of bond CPs and bond paths confirms the existence of the interaction (**Figure 14b**) since a bond CP and bond path connect the Ni atom to the H-atom. The supramolecular complex is further characterized by four bond CPs and bond paths connecting several H-atoms of the cationic fragment to the *i-mnt*$^{-2}$ ligand. The NBO analysis confirms the agostic nature of this interaction since only one orbital donor-acceptor interaction is found where the orbital of the σ(C–H) bond donates electrons to the empty d atomic orbital of Ni(II) with a concomitant stabilization energy of $E^{(2)}$ = 10.1 kJ/mol, thus confirming the importance of the agostic interaction.

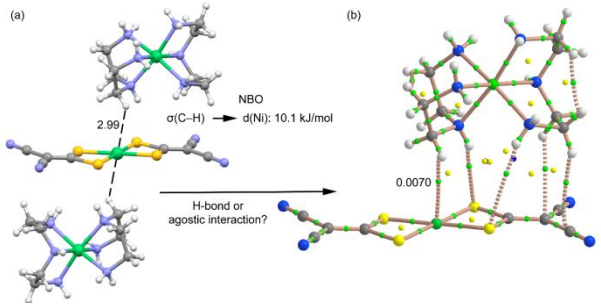

Figure 14. (a) X-ray fragment of compound **2** with indication of the C–H···Ni(II) interaction. Distance in Å. The result from the NBO calculations is also indicated. (b) Distribution of bond, ring and cage CPs (green, yellow and blue spheres, respectively) for a dimer extracted from the assembly. The value of ρ(r) at the bond CP is given in a.u.

In compound **3,** we have studied the intramolecular anion···π interaction that is established between the dianionic ligand and the *o*-phenylenediamine (**Figure 15a**). This interaction likely influences the shape of the polymeric chain. In principle the anion···π interactions is not favored in electron rich rings like *o*-phenylenediamine, however the coordination of the amino groups to the Ni(II) metal center increases the π-acidity of the ring. Since the solid state structure is polymeric, we have used a reduced theoretical model for the calculations (**Figure 15b**). The QTAIM analysis shows that indeed the S atom interacts with the π-system of the aromatic ligand (the bond path connects the S atom to one C atom of the ring). The NBO analysis shows that the interaction is very weak (in terms of orbital contribution) since the electron donation from the LP of the S atom to the antibonding π-orbital of one C=C bond is only $E^{(2)}$ = 1.42 kJ/mol in agreement with the small value of ρ(r) at the bond CP (0.0035 a.u.).

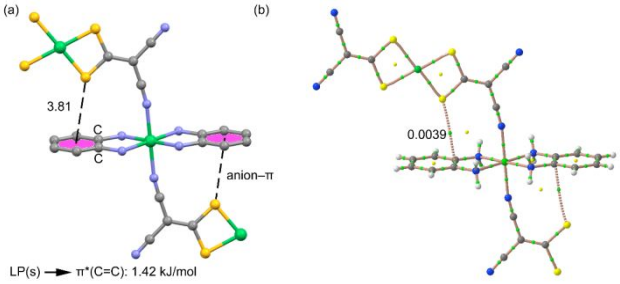

Figure 15. (a) X-ray fragment of compound **3** with indication of the anion–π interaction. Distance in Å to the ring centroid. The result from the NBO calculations is also indicated. (b) Distribution of bond and ring CPs (green and yellow spheres, respectively) for the dimer extracted from the assembly. The value of ρ(r) at the bond CP is given in a.u.

Electrochemical study

Cyclic Voltammetry was used to understand the behaviour of compounds **1**, **2** and **3** under reductive conditions. Solutions of all three compounds were prepared at a concentration of 0.1 mM in a 0.1 M acetonitrile solution of tetrabutylammonium hexafluorophosphate. A small sample of ferrocene (Fc) was added as an internal standard and scans were taken ranging in potential from -1.8 to +1 V using a glassy carbon working electrode, a platinum counter, and a silver reference. The resulting graphs were adjusted to the standard hydrogen electrode (SHE) by correcting for the position of the Fc^{+}/Fc redox couple [48]. Compounds **1**, **2** and **3** exhibit non-reversible reduction peaks at -1.62, -0.70 and -0.85 V vs the SHE respectively (**Figure 16**). Given that compounds **2** and **3** both contain square planar arrangements about a Ni center, it comes as no surprise that they are easier to reduce than the octahedral compound **1**. These two easier to reduce complexes are also shown to have greater catalytic ability for photocatalytic water reduction reactions.

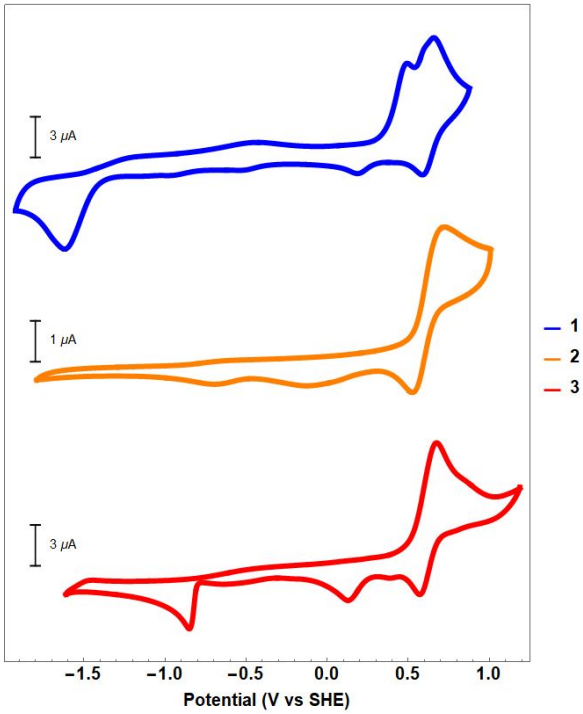

Figure 16. Cyclic voltammograms for compounds **1**, **2** and **3** taken in acetonitrile with potentials corrected to the SHE through the positioning of the Fc^{+}/Fc couple. Scale bars for the current for each scan are placed next to each scan indicating the current in micro-amps.

Catalytic study

Compounds **1**, **2**, and **3** were tested for their catalytic activity in a high throughput photoreactor measuring hydrogen evolution from an iridium photosensitized water reduction reaction. Use of this system enabled rapid screening over concentration ranges for the PS and the nickel species. Initial testing at a concentration range of 0.1 to 1.5 mM for the WRCs found that activity was greater at lower concentration, so the range of 0.01 to 0.1 mM was chosen for further testing (**Figure 17**). This range illustrates that these catalysts need little concentration to generate a substantial amount of hydrogen and are at their most active in this low range.

While all three compounds were highly active catalysts, compounds **2**, and **3**, which contain a square planar arrangement around nickel center(s), were found to be the most active, attaining turn over numbers (TON) of 1000 and 1119, respectively. Both values occurred at the lowest catalyst loading measured (0.01 mM), further indicating the potential for these systems to operate under ideal low loading conditions.

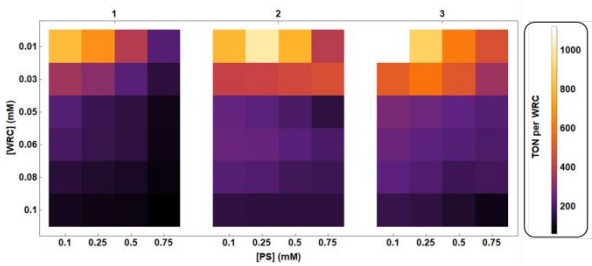

Figure 17. Catalytic activity in photocatalytic water reduction reactions using compounds **1**, **2**, and **3** at varying concentrations with $[Ir(Fmppy)_2dtbbpy\ PF_6]$ as PS. Reactions measured through photometric detection and results reported as turn over numbers (TON) based on the content of the WRC.

Conclusions

This work focuses on synthesis, supramolecular structural elucidation by X-ray diffraction and optimization by QTAIM, NBO, and HS analysis of Ni(II) complexes fabricated from dithiolate-polyamine based binary ligand systems and their catalytic activity in hydrogen evolution from iridium photosensitized water reduction reaction. The single crystal X-ray diffraction analysis reveal the direct impact of binary ligand systems on the coordination pattern of Ni(II) metal center imparting supramolecular arrangements involving discrete formation of square planar and octahedral geometries in **1**-**3**. In **1**, tripodal flexible chelate *tetraen* coordinated to Ni^{+2} in a trichelated fashion and *i-mnt*$^{-2}$ *via* thiolate ends revealing slightly distorted octahedral geometry and one solvent molecule (*DMSO*) disordered over two positions forms N H···O type hydrogen bonds imparting crystal stability. The secondary ligand *tren* influences the coordination modes of *i-mnt*$^{-2}$ to Ni^{+2} revealing square planar (NiS_4) and octahedral (NiN_6) geometries in the cocrystallised aggregates of **2,** where as in presence of *opda*, *i-mnt*$^{-2}$ behaves as S,S,N-tridentate connector forming 1D polymeric chains bearing consecutive square planar (NiS_4) and octahedral (NiN_6) coordination kernels. The significance of *DMF* solvent molecules lies in the fact that it forms 2D supramolecular chains *via* N3 H3A···O1 hydrogen bonds between parallel polymeric chains along *bc* plane imparting substantial stability to the crystal packing arrangement. All the hydrogen bonds in **1**-**3** are well corroborated by Hirshfeld surface analysis at molecular level. Except **1**, N···H/H···N interactions around 2.2 Å $<d_e+d_i<$ 2.8 Å predominates over S···H/H···S interactions around 2.4 Å $<d_e+d_i<$ 3.2 Å for all the coordination kernels that were examined separately by HS analysis. The same trend is further confirmed by HS analysis of Ni^{+2} metal centers. The data from 2D FP plots prove that apart from H···H and other minor contacts, hydrogen bond interactions account for more than 50% (**1**, 61.7%; **2A**, 86%; **2B**, 72%; **3A**, 86.1%; **3B**, 65.5%) of all the non-covalent contacts which act as driving force in supramolecular crystal packing. The Ni···H contact (3.5%) opens up the possibility of C H···Ni interaction (2.966 Å) between square planar (**2A**) and octahedral (**2B**) kernels in **2** which is further confirmed by QTAIM optimization. QTAIM and NBO optimizations at B3LYP/def2-TZVP level reveal the unorthodox interactions in the form of σ-hole chalcogen bonding interactions between cyano end of *i-mnt*$^{-2}$ and S-atom of *DMSO* in **1**, agostic interaction between σ(C–H) bond and empty d-orbital of Ni(II) with a concomitant stabilization energy of $E^{(2)}$ = 10.1 kJ/mol in **2**, and very weak anion···π interaction between LP of the thiolate-S atom and antibonding π-orbital of one C=C bond (phenyl ring of *opda*) [$E^{(2)}$ = 1.42 kJ/mol] in **3**. Applicability of **1**-**3** as highly active water reduced co-catalysts (WRC) in the photo-catalytic hydrogen evolution process is well proven from high turnover numbers (TON), (**2** and **3** are most active with TON 1000, 1119 respectively).

Author Contributions

Conflicts of interest

There are no conflicts to declare.

Acknowledgements

S.A acknowledges support from Govt. Degree College, Dharmanagar, Tripura (N)-799253, India. S.B. gratefully acknowledges National Science Foundation (NSF) funding CHE 1764353 for this work. Seed funding for the development of the high-throughput reactors came from Carnegie Mellon University's Manufacturing Futures Initiative. E.M.L. was supported by the Steinbrenner Institute Graduate Fellowship and the ARCS Foundation Pittsburgh Chapter. Seed code used to generate the image analysis program was provided by Tomasz Kowalewski. This research was supported by the U.S. Department of Energy, Office of Science, Office of Basic Energy Sciences, Data Science for Knowledge Discovery for Chemical and Materials Research program, under Award DE-SC0020392.

Notes and references

1. (a) P. Jayaraman, S. F. Ni and D. Li, *Coord. Chem. Rev*., 2020, **420**, 213398; (b) K. Tanifuji and Y. Ohki, *Chem. Rev.,* 2020, **120**, 5194; (c) M. Drosou, F. Kamatsos and C. A. Mitsopoulou, *Inorg. Chem. Front.,* 2020, **7**, 37; (d) R. R. Nasaruddin, T. Chen, N. Yan and J. Xie, *Coord. Chem. Rev.,* **2018**, **368**, 60.

2. (a) C. A. Bolos, A. T. Chaviara, D. Mourelatos, Z. Iakovidou, E. Mioglou, E. Chrysogelou and A. Papageorgiou, *Bioorg. Med. Chem*., 2009, **17 (35)**, 3142; (b) P. Deplano, L. Pilia, D. Espa, M. L. Mercuri and A. Serpe, *Coord. Chem. Rev.,* 2010, **254**, 1434; (c) G. Li, M. F. Mark, H. Lv, D. W. McCamant and R. J. Eisenberg, *J. Am. Chem. Soc.,* 2018, **140**, 2575; (d) M.R. Carlson, D.L. Gray, C.P. Richers, W. Wang, P.-H. Zhao, T.B. Rauchfuss, V. Pelmenschikov, C.C. Pham, L.B. Gee, H. Wang and S.P. Cramer, *Inorg. Chem*., 2018, **57**, 1988; (e) G. Cioncoloni, S. Sproules, C. Wilson and M. D. Symes, *Eur. J. Inorg. Chem*., 2017, 3707.

3. (a) T. Liu, W. Meng, Q.-Q. Ma, J. Zhang, H. Li, S. Li, Q. Zhao and Chen, *Dalton Trans.,* 2017, **46**, 4504; (b) Z. Chi, S. Takada, M. Kölzer, T. Matsumoto and K. Tatsumi, *Angew. Chem. Int. Ed*., 2006, *45*, 3768; (c) N. Yuan, C. Tian, T. Sheng, S. Hu and X. Wu, *Cryst. Growth Des.,* 2018, **18**, 5, 2667; (d) B. P. Biswal, H. A. Vignolo-González, T. Banerjee, L. Grunenberg, K. Gottschling, J. Nuss and B. V. Lotsch, *J. Am. Chem. Soc*., 2019, **141(28)**, 11082; (e) W. Zhang, J. Hong, J. Zheng, Z. Huang, J. Zhou and R. Xu, *J. Am. Chem. Soc.* 2011, **133**, 20680.

4. (a) H.S. Shafaat, O. Rudiger, H. Ogata and W. Lubitz, *Biochim. Biophys. Acta*., 2013, **1827**, 986; b) B.L. Greene, C.H. Wu, G.E. Vansuch, M.W. Adams and R.B. Dyer, *Biochemistry*, 2016, **55**, 1813.

5. (a) Z. Han, W. R. McNamara, M.-S. Eum, P. L. Holland and R. Eisenberg, *Angew. Chem., Int. Ed.,* 2012, **51**, 1667; (b) Z. Han, L. Shen, W. W. Brennessel, P. L. Holland and R. Eisenberg, *J. Am. Chem. Soc*., 2013, **135**, 14659.

6. (a) M. K. Singh, S. Sutradhar, B. Paul, S. Adhikari, F. Laskar, R. J. Butcher, S. Acharya and A. Das, *J. Mol. Struct*., 2017, **1139**, 395; (b) M. K. Singh, S. Sutradhar, B. Paul, S. Adhikari, F. Laskar,, S. Acharya, D. Chakraborty , S. Biswas, A. Das, S. Roy and A. Frontera, *J. Mol. Struct.*, 2018, **1139**, 334; (c) S. Adhikari, T. Bhattacharjee, P. Nath, A. Das, J. P. Jasinski, R. J. Butcher and D. Maiti, *Inorg. Chim. Acta.*, 2020, 119877; (d) S. Adhikari, T. Bhattacharjee, R. Gupta, C.-G. Daniliuc, M. Montazerozohori, R. Naghiha and A. Masoudiasl, *Polyhedron*, 2020, **192**, 114838; (e) S. Adhikari, T. Bhattacharjee, A. Das, S. Roy, C.-G. Daniliuc, J. K. Zaręba, A. Bauzá and Antonio Frontera, *CrystEngComm*, 2020, **22**, 8023; (f) T. Mochida, K. Takazawa, H. Matsui, M. Takahashi, M. Takeda, M. Sato, Y. Nishio, K. Kajita and H. Mori, *Inorg. Chem*., 2005, **44**, 8628.; (g) H. H. Alkam, A. Hatzidimitriou, C. C. Hadjikostas and C. Tsiamis, *Inorg. Chim. Acta.*, 1997, **256**, 41-50.

7. B. S. Kang, Z. N. Chen, C. Y. Su, Z. Lin and T. B. Wen, Polyhedron, 1998, 17, 2497.

8. (a) J. -M. Lehn, *Supramolecular Chemistry: Concepts and Perspectives*, VCH, Weinheim, 1995.; (b) M. Fujita, (ed.) *Molecular Self Assembly-Organic Versus Inorganic Approaches. Structure and Bonding*, **vol. 96**, Springer, Berlin, 2000; (c) S. Adhikari, D. Kar, R. Fröhlich and K. Ghosh, *ChemistrySelect*, 2019, **4**, 12825; (d) In-Won Park, J. Yoo, S. Adhikari, J. S. Park, J. L. Sessler and C. H. Lee, *Chem. Eur. J.,* 2012, **18**, 15073; (e) K. Ghosh, S. Adhikari. R. Frohlich, I. D. Petsalakis and G. Theodorakopoulos, *J. Mol. Struct*., 2011, **1004**, 193; (f) K. Ghosh, S. Adhikari and R. Frohlich, *Tetrahedron Letts*., 2008, **49**, 5063; (g) K. Ghosh and S. Adhikari, *Tetrahedron Letts*., 2006, **47**, 3577; (h) In- Won Park, J. Yoo, S. Adhikari, S. K. Kim, Y. Yeon, C. J. E. Haynes, J. L. Sutton, C. C. Tong, V. M. Lynch, J. L. Sessler, P. A. Gale and C.H. Lee, *Chem. Eur. J.,* 2012, **18**, 2514; (K) K. Ghosh, S. Adhikari, A. P. Chattopadhyay and P. R. Chowdhury, *Beilstein J. Org. Chem.*, 2008, **4**, 52.

9. (a) V. Mdluli, S. Diluzio, J. Lewis, J. F. Kowalewski, T. U. Connell, D. Yaron, T. Kowalewski and S. Bernhard, *ACS Catal.,* 2020, **10**, 6977; (b) I. N. Mills, J. A. Porras, J.A. and S. Bernhard, *Acc. Chem. Res.* 2018, **51**, 352; (c) J. H. Shon, S. Sittel, and T. S. Teets, *ACS Catal.,* 2019, **9**, 8646; (d) J. H. Shon and T. S. Teets, *Comments Inorg. Chem.,* 2020, **40**, 53-85.

10. (a) S. Metz and S. Bernhard, *Chem. Commun*., 2010, **46**, 7551; (b) P. N. Curtin, L. L. Tinker, C. M. Burgess, E. D. Cline and S. Bernhard, *Inorg Chem.*, 2009, **48**, 10498; (c) A. Fihri, V. Artero, A. Pereira and M. Fontecave, *Dalton Trans.,* 2008, 5567; (d) Y. Wang, X. Zhao, Y. Zhao, T. Yang, X. Liu, J. Xie, G. Li, D. Zhu, H. Tan and Z. Su, *Dyes and Pigments*, 2019, **170**, 107547.

11. (a) S. Diluzio, V. Mdluli, T. U. Connell, J. Lewis, V. VanBenschoten and S. Bernhard, *J. Am. Chem. Soc.* 2021, ASAP Article; (b) M. Yang, J. E. Yarnell, K. E. Roz, and F. N. Castellano, *ACS Appl. Energy Mater.,* 2020, **3**, 1842; (c) K. Dedeian, J. Shi, N. Shepherd, E. Forsythe and D. C. Morton, *Inorg. Chem.,* 2005, **44**, 4445; (d) S. Lamansky, P. Djurovich, D. Murphy, F. Abdel-Razzaq, H. E. Lee, C. Adachi, P. E. Burrows, S. R. Forrest and M. E. Thompson, *J. Am. Chem. Soc,* 2001, **123**, 4304; (e) F. Neve, M. La Deda,

A. Crispini, A. Bellusci, F. Puntoriero and S. Campagna, *Organometallics*, 2004, **23**, 5856.

12. (a) R. Henning, W. Schlamann and H. Kisch, *Angew. Chem. Int. Ed.,* 1980, **19**, 645; (b) E. Hontzopoulos, E. Vrachnou-Astra, J. Konstantatos and D. Katakis, *J. Photochem*. 1985, **30**, 117; (c) A. Das, Z. Han, W.W. Brennessel, P.L. Holland and R. Eisenberg, *ACS Catal.* 2015, **5**, 1397.
13. (a) J. Schneider, H.F. Jia, K. Kobiro, D.E. Cabelli, J.T. Muckerman and E. Fujita, *Energy Environ. Sci*. 2012, **5**, 9502; (b) B.J. Fisher and R. Eisenberg, *J. Am. Chem. Soc.* 1980, **102**, 361; (c) L.L. Efros, H.H. Thorp, G.W. Brudvig and R.H. Crabtree, *Inorg. Chem*., 1992, **31**, 1722.
14. (a) W. Zhang, J. Hong, J. Zheng, Z. Huang, J. Zhou and R. Xu, *J. Am. Chem. Soc.,* 2011, **133**, 20680; (b) H.H. Cui, J.Y. Wang, M.Q. Hu, C.B. Ma, H.M. Wen, X.W. Song and C.N. Chen, *Dalton Trans*., 2013, **42**, 8684; (c) H.N. Kagalwala, E. Gottlieb, G. Li, T. Li, R. Jin and S. Bernhard, *Inorg. Chem*., 2013, **52**, 9094.
15. K.A. Jensen and L. Henriksen, *Acta Chem. Scand.,* 1968, **22**, 1107.
16. R. W. W. Hooft, Bruker AXS, **2008**, Delft, The Netherlands.
17. Z. Otwinowski and W. Minor, *Methods Enzymol.,* 1997, **276**, 307.
18. Z. Otwinowski, D. Borek, W. Majewski and W. Minor, *Acta Crystallogr*., 2003, **A59**, 228.
19. G. M. Sheldrick, *Acta Cryst.,* 2015, **A71**, 3.
20. G. M. Sheldrick, *Acta Cryst.,* 2015, **C71 (1)**, 3.
21. M.A. Spackman and P.G. Byrom, *Chem. Phys. Lett.,* 1997, **267**, 215.
22. J.J. McKinnon, M.A. Spackman and A.S. Mitchell, *Acta Crystallogr*., 2004, **B60**, 627.
23. J.J. McKinnon, D. Jayatilaka and M.A. Spackman, *Chem. Commun.,* **2007**, 3814.
24. M.A. Spackman and D. Jayatilaka, *Cryst. Eng. Comm.,* 2009, **11**, 19.
25. M.J. Turner, J.J. McKinnon, S.K. Wolff, D.J. Grimwood, P.R. Spackman, D. Jayatilaka and M.A. Spackman, Crystal Explorer17, University of Western Australia, **2017**.
26. T. A. Keith, AIMAll (Version 13. 05.06), TK Gristmill Software, Overland Park KS, USA, **2013**.
27. M. J. Frisch, G. W. Trucks, H. B. Schlegel, G. E. Scuseria, M. A. Robb, J. R. Cheeseman, G. Scalmani, V. Barone, B. Mennucci, G. A. Petersson, H. Nakatsuji, M. Caricato, X. Li, H. P. Hratchian, A. F. Izmaylov, J. Bloino, G. Zheng, J. L. Sonnenberg, M. Hada, M. Ehara, K. Toyota, R. Fukuda, J. Hasegawa, M. Ishida, T. Nakajima, Y. Honda, O. Kitao, H. Nakai, T. Vreven, J. A. Montgomery, Jr., J. E. Peralta, F. Ogliaro, M. Bearpark, J. J. Heyd, E. Brothers, K. N. Kudin, V. N. Staroverov, R. Kobayashi, J. Normand, K. Raghavachari, A. Rendell, J. C. Burant, S. S. Iyengar, J. Tomasi, M. Cossi, N. Rega, J. M. Millam, M. Klene, J. E. Knox, J. B. Cross, V. Bakken, C. Adamo, J. Jaramillo, R. Gomperts, R. E. Stratmann, O. Yazyev, A. J. Austin, R. Cammi, C. Pomelli, J. W. Ochterski, R. L. Martin, K. Morokuma, V. G. Zakrzewski, G. A. Voth, P. Salvador, J. J. Dannenberg, S. Dapprich, A. D. Daniels, Ö. Farkas, J. B. Foresman, J. V. Ortiz, J. Cioslowski and D. J. Fox, Gaussian 09 (Revision B.01), Gaussian, Inc., Wallingford CT, **2009**.
28. (a) E.M. Lopato, E. A. Eikey, Z. C. Simon, S. Back, K. Tran, J. Lewis, J. F. Kowalewski, S. Yazdi, J. R. Kitchin, Z. W. Ulissi, J. E. Millstone and S. Bernhard, *ACS Catal*., 2020, **10**, 4244; (b) W. Song, W.; E.M. Lopato, S. Bernhard, P. A. Salvador and G. S. Rohrer, *Applied Catalysis B: Environmental,* 2020, **269**, 118750; (c) R. N. Motz, E.M. Lopato, T. U. Connell and S. Bernhard, *Inorg. Chem.*, 2021, ASAP Article.
29. P. N. Curtin, L. L. Tinker, C. M. Burgess, E. D. Cline and S. Bernhard, *Inorg. Chem*., 2009, **48**, 10498.
30. A. Grohmann and F. Knoch, *Inorg. Chem*., 1996, **35**, 7932.
31. R.M. Kirchner, C. Mealli, M. Bailey, N. Howe, L.P. Torre, L.J. Wilson, L.C. Andrews, N.J. Rose and E.C. Lingafelter, *Coord. Chem. Rev.,* 1987, **77**, 89.
32. L.J. Wilson and N.J. Rose, *J. Am. Chem. Soc.,* 1968, **90**, 6041.
33. J.E.K. Huheey, E.A. Keiter and R.L. Keiter, Inorganic Chemistry, Principles of Structure and Reactivity, Harper Collins, New York, **1993**, p. 482.
34. S. Adhikari, T. Bhattacharjee, R. J. Butcher, M. Porchia, M. De Franco, C. Marzano, V. Gandin and F. Tisato, *Inorg. Chim. Acta.*, 2019, **498**, 119098.
35. A. Okuniewski, D. Rosiak, J. Chojnacki and B. Becker, Polyhedron, 2015, **90**, 47.
36. S. Das, C.H. Hung and S. Goswami, *Inorg. Chem*., 2003, **42**, 8592.
37. A. Bondi, *J. Phys. Chem*., 1964, **68**, 441.
38. A. Castiñeiras, I. García-Santos, J. M. González-Pérez, A. Bauzá, J. K. Zaręba, J. Niclós-Gutiérrez, R. Torres, E. Vílchez and A. Frontera, *Cryst. Growth Des*., 2018, **18**, 6786.
39. G. Mahmoudi, J. K. Zaręba, A. Bauzá, M. Kubicki, A. Bartyzel, A. D. Keramidas, L. Butusov, B. Mirosław and A. Frontera, *Cryst. Eng. Comm*, 2018, **20**, 1065.
40. R. Banik, S. Roy, A. M. Kirillov, A. Bauza, A. Frontera, A. Rodriguez-Dieguez, J. M. Salas, W. Maniukiewicz, S. K. Das and S. Das, *Cryst. Eng. Comm*,. 2016, **18**, 5647.
41. G. Mahmoudi, J. K. Zaręba, A. V. Gurbanov, A. Bauzá, F. I. Zubkov, M. Kubicki, V. Stilinović, V. Kinzhybalo and A. Frontera, *Eur. J. Inorg. Chem*., 2017, 4763.
42. A.Y. Meyer, *J. Comput. Chem*., 1986, **7**, 144.
43. J. Rudnick and G. Gaspari, *J. Phys. a – Mathemat*., 1986, **19**, 191.
44. Y. S. Tan, A. Otero-de-la-Roza, M. M. Jotani and E. R. T. Tiekink, *Cryst. Growth Des*., 2020, **20**, 3272.
45. C. B. Pinto, L. H. R. D. Santos and B. L. Rodrigues, *Cryst. Growth Des*. 2020, **20**, 4827.
46. E. D. Glendening, C. R. Landis and F. Weinhold, *WIREs Comput. Mol. Sci*., 2012, **2**, 1.
47. F. Weinhold and C. R. Landis, Valency and bonding: a natural bond orbital donor-acceptor perspective, Cambridge University Press, Cambridge, UK, **2005.**
48. V. V. Pavlishchuk, A. W. Addison; Conversion constants for redox potentials measured versus different electrodes in acetonitrile solutions at 25°C. *Inorganica Chimica Acta*, **2000**, *298*, 97-102.